Calculation of photoelectron spectra: A mean-field-based scheme

P. M. Dinh,[1,2] P. Romaniello,[1,3] P.-G. Reinhard,[4] and E. Suraud[1,2]
[1]*CNRS, LPT (IRSAMC) F-31062 Toulouse, France*
[2]*Université de Toulouse, UPS, Laboratoire de Physique Théorique (IRSAMC) F-31062 Toulouse, France*
[3]*European Theoretical Spectroscopy Facility (ETSF)*
[4]*Institut für Theoretische Physik, Universität Erlangen, D-91058 Erlangen, Germany*
(Received 18 June 2012; published 21 March 2013)

In a previous work, Pohl *et al.* [Phys. Rev. Lett. **84**, 5090 (2000)] have proposed a simple scheme for the evaluation of photoelectron spectra of clusters subject to a laser field by collecting one-particle wave functions at a given measuring point close to absorbing boundaries. The scheme gives reliable results for low and moderate laser fields, but it shows failures for strong laser fields. The formulation relies on the assumption of free-electron propagation close to the boundaries. The laser field, however, can still be active when the first bunches of outgoing electrons reach the measuring point, and therefore the free-particle scenario may not hold anymore in case of high laser intensities. In this paper, hence, we generalize the method by using a model of "free" particles in the presence of an electromagnetic dipole field. Numerical tests show that this generalized scheme reduces to that of Pohl *et al.* for low and moderate laser intensities, whereas it considerably improves the results of the latter for high intensities, thus extending the applicability of the method.

DOI: 10.1103/PhysRevA.87.032514 PACS number(s): 33.60.+q, 33.80.Eh, 36.20.Kd

I. INTRODUCTION

Photoelectron spectra (PES) constitute a long-standing basic tool for analyzing the electronic structure of atoms, molecules, or solids [1–3]. In the one-photon regime, PES provide an image of the sequence of single-particle levels which are occupied in the ground state. This has been applied, e.g., already in the early days of cluster physics to the electronic structure of cluster anions to track the transition to bulk metal [4]. Whereas this could be done with photon frequencies in the range of visible light, the analysis of deeper levels requires higher frequencies, and hence one finds also UV [5] and x-ray PES [6]. Nowadays, we dispose of a great variety of coherent light sources in large ranges of frequency, intensity, and pulse length, such as the very powerful and versatile free-electron lasers [7,8], which now even allow for time-resolved studies of deeply lying core states of atoms embedded in a material [9]. With the great availability of good light sources, studies of PES are now found in all areas of molecular physics, from atoms over simple molecules [10] to complex systems as clusters [11] and organic molecules [12]. In turn, PES now offer a remarkable tool of investigation of both structural and dynamical properties of these various atomic systems.

There is hence a general need for a robust theoretical tool of analysis of PES in various dynamical regimes. Traditional approaches to compute PES rely on (multi)photon perturbation theory [13] which is naturally limited to low laser intensities. A method employing directly fully fledged time-dependent density-functional theory has been developed a few years ago in Refs. [14,15] and has been taken up recently in Ref. [16] for a combined analysis of PES and angular distributions of emitted electrons. Here, the PES are deduced directly from numerical simulations of the electronic excitations on a spatial grid representation allowing exploration of a rather wide range of dynamical scenarios. The technique has been applied to a variety of systems for which significant electron emission can be achieved with still moderate laser intensities such as free metal clusters [17–19], dimer molecules [16], and clusters deposited on substrate [20]. However, when high laser intensities are employed, as often in case of atoms and molecules with large ionization potentials, the method can produce unphysical features in the PES. The focus of this work is hence on generalizing the scheme of Refs. [14,15] to also treat high laser intensities but, at the same time, still keeping the simplicity of the framework.

The paper is organized as follows. We start in Sec. II A with a brief review of the original scheme to evaluate PES as proposed in Ref. [14]. Using the example of the Na_9^+ cluster in a strong laser field, we show that this scheme produces unexpected spectral features in the PES which call for a revision of the method. A generalized scheme is hence proposed, which is based on the solution of the time-dependent Schrödinger equation for a particle in the presence of a homogeneous laser field. This implies that we also discuss the gauge freedom in describing the laser field and which gauge is most appropriate for the evaluation of PES. The generalized scheme is then tested in Sec. III for the analytically solvable case of Gaussian wave packets first and then numerically for a few realistic test cases. The tests show that the present scheme reduces to the original scheme of Ref. [14] in the case of low and moderate laser intensities, whereas it greatly improves the results of the latter for high laser intensities. We end the paper with our conclusions and future perspectives.

II. THEORETICAL EVALUATION OF PES

In this section, we first give a brief review of the scheme for the evaluation of PES introduced in Refs. [14,15]. After showing that it is not appropriate for high laser intensities, we propose a generalized scheme that solves the problem. All schemes discussed here and in the previous papers rely on a mean-field description where each electron is associated with a single-electron wave function ψ_α. We will consider in the formal discussions one representative state and drop the index α to simplify notations. Moreover, for sake of simplicity, the derivations are done for one-dimensional (1D) systems; the

generalization to three dimensions (3D) is straightforward and is detailed in Appendix A.

A. PES scheme for free particles

The PES are efficiently calculated by exploiting the features of the absorbing boundary conditions [14,15]. We choose a "measuring point" $z_{\mathcal{M}}$ far away from the center and one or two grid points before the absorbing boundaries. In the region around $z_{\mathcal{M}}$, we will assume a free-electron dynamics; each electron is then described by the single-electron wave function $\psi(z,t)$, which can be considered as a superposition of plane waves. The ψ is recorded at the measuring point $z_{\mathcal{M}}$ during the time evolution. This delivers the raw information from which we extract the PES. We give here a brief summary of the procedure and its motivations.

1. Direct evaluation scheme

The conceptually simplest access to PES proceeds similar to the experimental setup. The measurement of PES is practically a momentum analysis of the outgoing wave packet at a remote side (see, e.g., [21] and references therein). To map this situation into a theoretical scheme, one assumes that one has a very large numerical grid and a spatial momentum analyzer far away from the cluster region. This analyzing region covers a sufficient span of spatial extension to allow definition of a momentum in coordinate space. The cluster's mean field becomes negligible in this region. If one assumes that here also the laser field is negligible, then one encounters free-particle dynamics. This is governed by the time-dependent Schrödinger equation for a free particle $\mathrm{i}\partial_t \psi(z,t) = -\frac{\nabla^2}{2}\psi(z,t)$, whose solution is

$$\psi(z,t) = \int \frac{dk}{\sqrt{2\pi}}\, \widehat{\psi}_0(k)\, e^{i(kz-\omega_k t)}, \quad \omega_k = \frac{k^2}{2}. \tag{1}$$

Atomic units $\hbar = m_e = e = 4\pi\epsilon_0 = 1$ are used here and throughout the paper. The momentum components $\widehat{\psi}_0(k)$ carry the wanted information on the distribution of kinetic energies ω_k. They are filtered by inverse Fourier transformation in coordinate space:

$$\widehat{\psi}(k,t) = \int \frac{dz}{\sqrt{2\pi}} e^{-ikz}\psi(z,t) = \widehat{\psi}_0(k)e^{-i\omega_k t}. \tag{2}$$

In fact, the z integration has to be confined in principle to the analyzer region which limits the resolution. We can assume that the region is still large enough in practice to deliver sufficient resolution. The probability to find an outgoing particle with momentum k is then given by $|\widehat{\psi}(k,t)|^2 = |\widehat{\psi}_0(k)|^2$. Only outgoing particles reach the analyzing volume such that the momentum has a unique sign $k > 0$ which provides a one-to-one correspondence of k and the kinetic energy $E_{\mathrm{kin}} \equiv \omega_k$. The PES can thus be obtained as

$$\mathcal{Y}(E_{\mathrm{kin}}) \propto \frac{1}{\sqrt{E_{\mathrm{kin}}}}|\widehat{\psi}_0(k)|^2, \tag{3}$$

where the appropriate energy density $\propto E_{\mathrm{kin}}^{-1/2}$ is taken into account. We call this method, built in analogy to the experimental setup, the "direct scheme."

2. Frequency analysis at measuring point

The direct scheme, although conceptually simple, is inapplicable in realistic cases because it requires huge numerical boxes and long computation times. This is because we would need a large extra space for the spatial Fourier analysis. To overcome this problem, we recover the momentum distribution, and with it the PES, from the Fourier transform into the frequency domain

$$\widetilde{\psi}(z_{\mathcal{M}},\omega) = \int \frac{dt}{\sqrt{2\pi}}\, e^{i\omega t}\psi(z_{\mathcal{M}},t). \tag{4}$$

We insert the free wave packet (1) for $\psi(z_{\mathcal{M}},t)$ and obtain

$$\begin{aligned}\widetilde{\psi}(z_{\mathcal{M}},\omega) &= \int \frac{dk}{\sqrt{2\pi}}\, e^{ikz_{\mathcal{M}}} \int \frac{dt}{\sqrt{2\pi}}\, e^{i(\omega-\omega_k)t}\widehat{\psi}_0(k) \\ &= \int dk\, e^{ikz_{\mathcal{M}}}\, \delta(\omega-\omega_k)\widehat{\psi}_0(k) \\ &= \int \frac{dk}{k}\, e^{ikz_{\mathcal{M}}}\, \delta(k-\sqrt{2\omega_k})\widehat{\psi}_0(k) \\ &= \frac{\widehat{\psi}_0(\sqrt{2\omega_k})}{\sqrt{2\omega_k}}\, e^{iz_{\mathcal{M}}\sqrt{2\omega_k}},\end{aligned} \tag{5}$$

where we exploited the fact that $k > 0$ to allow the unique correspondence $k = \sqrt{2\omega_k}$. From Eq. (5), it becomes clear that we can use $\widetilde{\psi}(z_{\mathcal{M}},\omega)$ in place of $\widehat{\psi}_0(k)$ to calculate the PES. Again, we identify $E_{\mathrm{kin}} \equiv \omega_k$ and obtain the PES yield $\mathcal{Y}_{z_{\mathcal{M}}}(E_{\mathrm{kin}})$ as

$$\mathcal{Y}_{z_{\mathcal{M}}}(E_{\mathrm{kin}}) \propto \sqrt{E_{\mathrm{kin}}}|\widetilde{\psi}(z_{\mathcal{M}},E_{\mathrm{kin}})|^2. \tag{6}$$

Equation (6) is the scheme originally proposed in Refs. [14,15]. We have checked the method in extensive 1D wave-packet calculations and compared it to the "direct" scheme (3). Both methods yield the same results, while the above-sketched frequency analysis at a "measuring point" is orders of magnitude faster. We call this scheme deduced from frequency analysis the "raw recipe" to distinguish it from the generalized case presented later on.

The above derivation was done for the case of one spatial dimension. The same steps can be done for three-dimensional wave packets (for details, see Appendix A) leading to a yield $\propto|\widetilde{\psi}(\mathbf{r}_{\mathcal{M}},E_{\mathrm{kin}})|^2$.

3. Example of application and problem

Although the simple scheme based on Eq. (6) has been applied with success to a variety of dynamical scenarios in clusters, our recent attempts to compute the PES of small covalent organic molecules have raised some questions concerning its general applicability. For high laser intensities, we find an unexpected shoulder in the PES at large kinetic energies. These patterns were then also found for the simple test case of Na_n clusters with jellium background when going to sufficiently large laser field strengths. This excludes pseudopotentials, local or nonlocal ones, as the source of the trouble. The problem seems to reside in the scheme to evaluate the PES.

Figure 1 demonstrates the problem for the case of Na_9^+. The spherical jellium model is used for the ionic background.

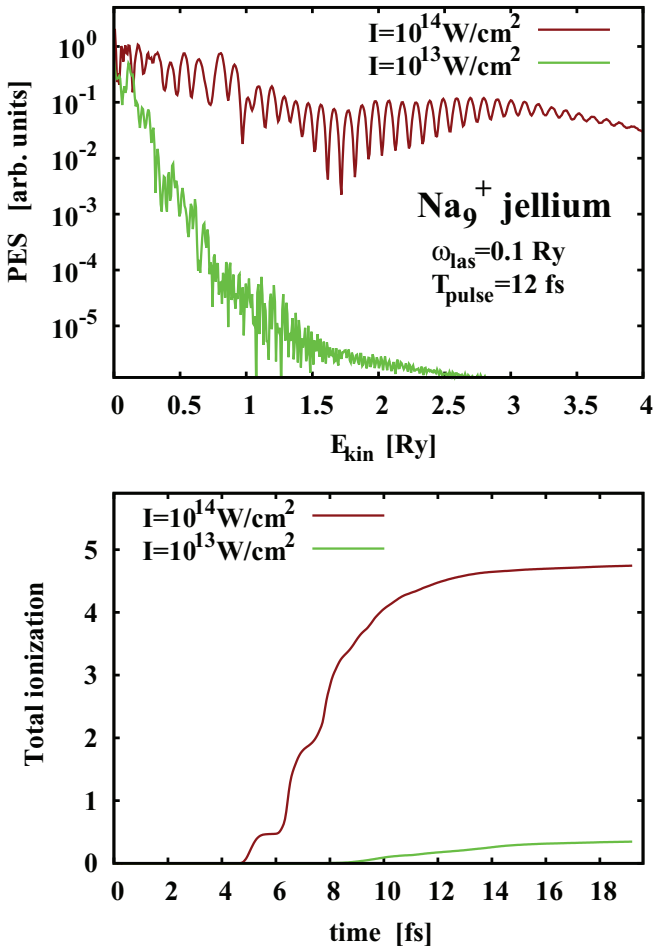

FIG. 1. (Color online) Ionization properties of Na_9^+ with jellium background under the influence of laser pulses having frequency $\omega_{las} = 0.1$ Ry, pulse length $T_{pulse} = 12$ fs, and intensities $I = 10^{13}$ W/cm^2 (green or light gray lines) and $I = 10^{14}$ W/cm^2 (brown or dark gray lines), computed in a cylindrical box of $176 \times 88a_0^2$ with spherical absorbing bounds covering at least 16 grid points. The laser field was given effectively in the v gauge. Bottom: time evolution of ionization. Top: photoelectron spectra $\mathcal{Y}_{\Omega_{\mathbf{r}_\mathcal{M}}}(E_{kin})$ [see Eq. (A3)].

Valence electrons are described by the time-dependent local-density approximation (TDLDA) using the energy functional of Ref. [22] and an average-density self-interaction correction (ADSIC) [23]. Two cases are considered for comparison: one with still moderate laser intensity ($I = 10^{13}$ W/cm^2), and another one in the high intensity regime ($I = 10^{14}$ W/cm^2). In the latter regime, more than half of the cluster's electrons are stripped off, as shown in the bottom panel of Fig. 1. The top panel shows the PES for both cases. For a moderate intensity I, it is already seen that the multiphoton peaks are washed out [14]. What remains is the typical monotonous decrease. The case of high intensity differs: up to $E_{kin} \approx 1.8$ Ry, we see the typical pattern of a monotonous decrease of the envelope with some fluctuations. For $E_{kin} > 1.8$ Ry, however, we observe a new maximum, a broad shoulder of high-energy electrons; this is unexpected and most probably unphysical. In the following, we clarify the origin of such a shoulder and we generalize the method to compute PES to a wider range of laser intensities.

B. PES scheme for free particles plus laser field

In Sec. II A, we have deduced the recipe for evaluating PES under the assumption that the potential is negligible at the measuring point. Although this may hold for the typical mean field of a system, we can not easily exclude the presence of the laser field at this point because the laser field is of extremely long range (wavelength much larger than system size in the dipole approximation that we use here). Of course, one could take very large boxes, so that the laser would have died at a time when the emitted electrons reach the measuring point $z_\mathcal{M}$. This would avoid a temporal overlap between the laser and the collected outgoing wave and validate the simple recipe. However, this would enormously increase the computational time, if not inhibit a calculation at all. We have hence to deal with the situation where the laser is still active at the measuring point. To do this, we extend the above considerations to the case of a "free" particle plus laser field in the dipole approximation. This is still analytically solvable and leads to a generalized scheme using a simple phase correction. We again confine the considerations to the 1D case. The extension to 3D is straightforward.

1. Hamiltonian and choice of the gauge

We are now considering a free electron in the presence of an external electromagnetic field governed by the Hamiltonian

$$\hat{H}(\mathbf{r},t) = \frac{1}{2}\left[\hat{\mathbf{p}} + \frac{\mathbf{A}(\mathbf{r},t)}{c}\right]^2 - \Phi(\mathbf{r},t), \tag{7}$$

where $\mathbf{A}$ is the vector potential and Φ the scalar potential. The external laser field is described in the limit of long wavelengths and neglecting magnetic effects (electronic velocities are very small at any time). There remains the gauge freedom in choosing $\mathbf{A}$ and Φ. Most commonly used are the *space gauge* (x gauge) and the *velocity gauge* (v gauge). In the former one, the laser field is described, within the dipole approximation, by a scalar potential only:

$$\mathbf{A}^{(x)}(\mathbf{r},t) = \mathbf{0}, \quad \Phi^{(x)}(\mathbf{r},t) = -E_0 f(t) z. \tag{8}$$

The laser polarization is chosen here along the z axis, E_0 is the maximum field amplitude, and $f(t)$ denotes the carrier envelope of the laser pulse. In the *velocity gauge* instead, the laser field enters the Hamiltonian as a vector potential only:

$$\mathbf{A}^{(v)}(\mathbf{r},t) = -cE_0 F(t)\,\mathbf{e}_z, \quad \Phi^{(v)}(\mathbf{r},t) = 0, \tag{9}$$

$$F(t) = \int_{-\infty}^{t} dt'\, f(t'). \tag{10}$$

Note that the vector potential in dipole approximation is spatially constant. Both gauges are equivalent. They are connected by a gauge transformation (for details, see Appendix B).

If there is no temporal overlap between laser signal and outgoing wave at $z_\mathcal{M}$, then each gauge produces the same results for the PES. However, in case of overlap, the choice of gauge becomes relevant. One of the goals of this paper is to identify which gauge is most suitable for evaluating PES.

2. Solution of the Schrödinger equation with field

We start from the Schrödinger equation of a free particle with the external field in v gauge [see Eq. (9)], which provides the simplest analytical solution. It reads as, in momentum space,

$$\tfrac{1}{2}[k - E_0 F(t)]^2\, \widehat{\psi}^{(v)}(k,t) = i\, \partial_t \widehat{\psi}^{(v)}(k,t),$$

for which the solution is

$$\widehat{\psi}^{(v)}(k,t) = \exp(-i\omega_k t + ik\delta q - i\delta\Omega)\, \widehat{\psi}_0^{(v)}(k), \tag{11a}$$

with

$$\omega_k = \frac{k^2}{2}, \tag{11b}$$

$$\delta q(t) = E_0 \int_0^t dt'\, F(t'), \tag{11c}$$

$$\delta\Omega(t) = \frac{E_0^2}{2} \int_0^t dt'\, F(t')^2. \tag{11d}$$

Through the gauge transformation (B3) (see Appendix B), the solution of the Schrödinger equation in the x gauge can be easily obtained from the solution (11a) in the v gauge as

$$\widehat{\psi}^{(x)}(k,t) = \exp(-i\omega_K t + iK\delta q - i\delta\Omega)\, \widehat{\psi}_0^{(v)}(k), \tag{12a}$$

with

$$K = k + E_0 F(t), \tag{12b}$$

$$\omega_K = \frac{K^2}{2}, \tag{12c}$$

where δq and $\delta\Omega$ are given in Eqs. (11c) and (11d), respectively.

Before proceeding, one should note that the gauge transformation allows one to decouple the gauge used in the analysis from that used in the dynamical solution. In practice, the x gauge is more efficient in dynamical propagation since the field operator (8) in the x gauge is purely local.

3. Direct evaluation scheme

One can easily verify that when the PES is calculated using the direct evaluation scheme, i.e., in terms of the wave function in momentum space, both (11a) and (12a) deliver the same result displayed in Eq. (3). As mentioned above, this scheme is computationally too expensive; we will hence extract the needed information from the wave function in frequency space, as illustrated in the following.

4. Frequency analysis at the measuring point

We start from the solution of the Schrödinger equation for an electron in a laser field in the v gauge. The wave function being sampled then reads as $\psi^{(v)}(z_{\mathcal{M}},t) = \int \frac{dk}{\sqrt{2\pi}}\, e^{ikz_{\mathcal{M}}}\, \widehat{\psi}_0^{(v)}(k)\, e^{-i\omega_k t + ik\delta q - i\delta\Omega}$. Trying to directly apply the time-frequency transformation runs into trouble due to the nontrivial time dependencies induced by the factors $\delta q(t)$ and $\delta\Omega(t)$. A solution is simply to counterweight the disturbing phase factors by a phase-correction factor $e^{i\varphi}$ before the transformation. The PES is then calculated from the frequency Fourier transform of this "phase-augmented" (PA) wave function

$$\widetilde{\psi}^{(\mathrm{PA})}(z_{\mathcal{M}},\omega) = \int \frac{dt}{\sqrt{2\pi}}\, e^{i\omega t} e^{i\varphi} \psi^{(v)}(z_{\mathcal{M}},t), \tag{13a}$$

with the phase

$$\varphi(t) = -\sqrt{2\omega}\, \delta q(t) + \delta\Omega(t). \tag{13b}$$

This wave function will deliver an approximate PES, as it can be understood from the following analysis. By inserting the k-space solution (11a), one can express the wave function (13a) as

$$\begin{aligned}\widetilde{\psi}^{(\mathrm{PA})}(z_{\mathcal{M}},\omega) &= \int \frac{dt}{\sqrt{2\pi}}\, e^{i[\omega t - \sqrt{2\omega}\,\delta q(t) + \delta\Omega(t)]} \int \frac{dk}{\sqrt{2\pi}} \exp[-i\omega_k t + ik\delta q(t) - i\delta\Omega(t) + ikz_{\mathcal{M}}]\, \widehat{\psi}_0^{(v)}(k) \\ &= \int \frac{dk}{\sqrt{2\pi}}\, e^{ikz_{\mathcal{M}}} \widehat{\psi}_0^{(v)}(k) \underbrace{\int \frac{dt}{\sqrt{2\pi}} \exp[-i(\omega - \omega_k)t + i(k - \sqrt{2\omega})\delta q(t)]}_{D(\omega,k)}.\end{aligned}$$

Further analytical evaluation is hindered by the time dependence of $\delta q(t)$. For a rough estimate of its effects, we consider the Taylor expansion $\delta q(t) \approx \delta q' t + \delta q'' t^2/2 + \cdots$. At first order in t, we obtain $D(\omega,k) = \delta(\omega - \frac{k^2}{2} + (k - \sqrt{2\omega})\delta q')$, which can be resolved to $k = \sqrt{2\omega}$; for higher orders, this is not strictly the case anymore. One gets, therefore, only an approximate relation $k \approx \sqrt{2\omega}$, or $E_{\mathrm{kin}} = \omega$ equivalently. This suggests that the PES can be calculated as

$$\mathcal{Y}_{z_{\mathcal{M}}}(E_{\mathrm{kin}}) \propto \sqrt{E_{\mathrm{kin}}}\, \left|\widetilde{\psi}^{(\mathrm{PA})}(z_{\mathcal{M}}, E_{\mathrm{kin}})\right|^2. \tag{14}$$

Our tests show that this is reliable for moderate field strengths and/or slow field oscillations, whereas it fails for too strong or too quickly oscillating fields.

The additional move in this generalized evaluation is to augment the original recipe by the phase-correction factor $e^{i\varphi}$. The factor becomes negligible for weak laser fields, or for fields which do not interfere in time with the emitted particle flow; it becomes, instead, important in the other cases. As will be demonstrated in the next section, this allows us to apply the recipe in a wider range of laser intensities and carrier envelopes. In order to distinguish it from the original scheme (6), coined the "raw" scheme, we call the generalized form (14) the "phase-augmented" (PA) scheme.

We run into insurmountable trouble if we try to develop a generalized scheme on the basis of the solution (12a) in the x gauge because here even the instantaneous momentum K, as given in Eq. (12b), depends on time. This is another strong

$$\begin{array}{lll}
\text{Direct recipe} & : \text{Compute } \psi(z_{\mathcal{M}},t) \xrightarrow{k-\mathrm{FT}} \widehat{\psi}(k,t) & \longrightarrow \mathcal{Y} = \dfrac{1}{\sqrt{E_{\mathrm{kin}}}}\left|\widehat{\psi}(k,t)\right|^2 = \dfrac{1}{\sqrt{E_{\mathrm{kin}}}}\left|\widehat{\psi}_0(k)\right|^2 \\
\text{Raw recipe in } v\text{−gauge} & : \text{Compute } \psi^{(x)}(z_{\mathcal{M}},t) \xrightarrow{\text{gauge transf.}} \psi^{(v)}(z_{\mathcal{M}},t) \xrightarrow{\omega-\mathrm{FT}} \widetilde{\psi}^{(v)}(z_{\mathcal{M}},\omega) & \longrightarrow \mathcal{Y}_{z_{\mathcal{M}}} = \sqrt{E_{\mathrm{kin}}}\left|\widetilde{\psi}^{(v)}(z_{\mathcal{M}},\omega)\right|^2 \\
\text{PA recipe in } v\text{−gauge} & : \quad \psi^{(v)}(z_{\mathcal{M}},t) \xrightarrow{\mathrm{PA}} e^{i\varphi}\psi^{(v)}(z_{\mathcal{M}},t) \xrightarrow{\omega-\mathrm{FT}} \widetilde{\psi}^{(\mathrm{PA})}(z_{\mathcal{M}},\omega) & \longrightarrow \mathcal{Y}_{z_{\mathcal{M}}} = \sqrt{E_{\mathrm{kin}}}\left|\widetilde{\psi}^{(\mathrm{PA})}(z_{\mathcal{M}},\omega)\right|^2
\end{array}$$

FIG. 2. Summary of the recipes for the reconstruction of photoelectron spectra discussed in this paper. "FT" stands for "Fourier transformation".

indication that the v gauge is the appropriate starting point for evaluating the PES (as was already argued in Refs. [14,24]). This will be confirmed in the next section with a practical example.

We summarize the different recipes for the reconstruction of PES explored in this paper in Fig. 2. Note that the wave functions are written in 1D. Mind also that the k transform is to be taken over a large interval on a remote site.

III. TEST OF THE GENERALIZED SCHEME

In this section, we test the performance of the generalized scheme (14). We first apply it to an exactly solvable model (free Gaussian wave packet), and then to the more realistic case of a Na_9^+ cluster. In both cases, we consider the temporal profile $f(t)$ of the laser pulse in the form

$$f(t) = \sin(\omega_{\mathrm{las}}t)\sin^2\left(\frac{\pi\, t}{T_{\mathrm{pulse}}}\right)\theta(t)\,\theta(T_{\mathrm{pulse}}-t), \qquad (15)$$

where ω_{las} is the laser frequency, T_{pulse} the duration of the laser pulse, and θ denotes the Heaviside function. We have chosen for the envelope a smooth $\sin^2$ profile which combines high spectral selectivity and finite extension.

A. Analytical test case: Gaussian wave packet

As a first test case, we consider a Gaussian wave packet whose propagation can be described analytically, even in the presence of a (homogeneous) laser field (see Appendix C). The analytical solution, carried forth to far distance and beyond the lifetime of the laser field, allows a direct (and exact) evaluation of the PES by filtering the momentum components by Fourier transformation from coordinate to momentum space, according to Eq. (3). Thus, we can test the PES analysis in frequency space, namely the raw scheme (6) and the PA scheme (14), against the exact result given by the direct scheme (3). In the following, we analyze three different scenarios: (i) low laser intensity and overlap between laser pulse and flow signal at the measuring point; (ii) high laser intensity and overlap between laser pulse and flow signal at the measuring point; (iii) high laser intensity and no overlap between laser pulse and flow signal at the measuring point.

1. *Evaluation of PES with the direct scheme*

We consider a one-dimensional system with a Hamiltonian consisting of the free kinetic energy plus the external laser field, as it was discussed in Sec. II B. The initial wave function reads as, in momentum space,

$$\widehat{\psi}_0(k) = \left(\frac{\mu_0}{\pi}\right)^{1/4} e^{iq_0(p_0-k)}\exp\left(-\frac{\mu_0}{2}(k-p_0)^2\right). \qquad (16)$$

Propagation in the laser field as given by Eq. (11a) is described through a time-dependent phase factor which reduces to the trivial $\exp(-i\omega_k t)$ once the laser pulse is over. Such a phase factor is irrelevant for the spatial Fourier transformation. Thus, the direct evaluation (3) yields the PES

$$\begin{aligned}
\mathcal{Y}(E_{\mathrm{kin}}) &\propto \sqrt{\frac{1}{E_{\mathrm{kin}}}}\,|\widehat{\psi}_0(\sqrt{2E_{\mathrm{kin}}})|^2 \\
&= \sqrt{\frac{1}{E_{\mathrm{kin}}}}\left(\frac{\mu_0}{\pi}\right)^{1/2} e^{-\mu_0(\sqrt{2E_{\mathrm{kin}}}-p_0)^2}. \qquad (17)
\end{aligned}$$

2. *Evaluation of PES with the phase-augmented scheme*

The phase-augmented analysis of PES can be worked out analytically, along the line shown in Eq. (13a), which yields the exact result (17). For a more practical test, we have computed the wave packet in coordinate space explicitly as $\psi^{(x)}(z_{\mathcal{M}},t)$ or $\psi^{(v)}(z_{\mathcal{M}},t)$ and applied the raw as well as the phase-augmented analysis numerically.

We use a wave packet with the following parameters: $p_0 = 1a_0^{-1}$, $q_0 = 0$, $\mu_0 = 100\ a_0$. This roughly mocks up the spatial extension (about 10 a_0) of a typical electronic wave function in a moderate size (some tens of atoms) sodium cluster. The associated momentum p_0 in turn typically corresponds to about twice the Fermi momentum in such systems, thus again typical of the dynamics of laser irradiation scenario.

For the laser pulse [Eq. (15)], we take $\omega_{\mathrm{las}} = 0.11$ Ry $= 1.4$ eV, $T_{\mathrm{pulse}} = 8000\ \mathrm{Ry}^{-1} = 384$ fs, and various field strengths E_0 where the relation between E_0 and laser intensity is $I = 10^{14}$ W/cm^2 $\leftrightarrow E_0 = 0.109$ Ry/a_0, $I = 10^{12}$ W/cm^2 $\leftrightarrow E_0 = 0.0109$ Ry/a_0, $I = 10^{10}$ W/cm^2 $\leftrightarrow E_0 = 0.00109$ Ry/a_0. The measuring point was taken at $z_{\mathcal{M}} = 1000\ a_0$ or $2000\ a_0$. The first choice yields a temporal overlap between laser pulse and flow signal at $z_{\mathcal{M}}$, whereas the second choice decouples them.

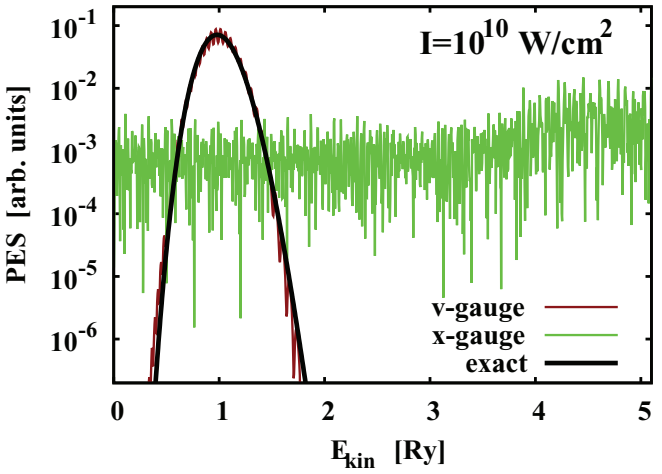

FIG. 3. (Color online) Photoelectron spectra from wave-packet analysis for a weak intensity $I = 10^{10}$ W/cm^2. We use the raw scheme (6) and compare analysis from the wave function in the v (brown or dark curve) and x gauge (green or light gray line). The direct evaluation of PES from momentum distribution of the wave packet as given in Eq. (17) is also shown (black thick line).

3. Low intensity, temporal overlap with laser pulse

The case of low intensity and overlap of wave packet with laser pulse at the measuring point is illustrated in Fig. 3, where we compare the evaluation of PES for the x gauge versus the v gauge for a case of weak laser field where the phase correction φ in Eq. (13a) is negligible such that we can effectively use the "raw recipe" (6). It becomes clear that the result from the wave function in the x gauge is unphysical. The source of the problem lies in the extra contribution $\exp[iE_0F(t)z_{\mathcal{M}}]$ in the wave function in the x gauge [see Eq. (B3)]. As soon as the momentum $p = p(t)$ changes even slightly in time, the possibly large $z_{\mathcal{M}}$ can amplify such a small oscillation and induce dramatic phase oscillations which, in turn, produce a large contribution to the PES. This contribution, however, must be unphysical because it sensitively depends on the choice of the measuring point. Clearly, the v gauge is the preferred choice for the evaluation of PES. This was already expected from the analytical considerations in Sec. II B4. We will henceforth exclusively use the v gauge. Of course, a numerical solution of the Schrödinger equation in coordinate space is often much simpler in the x gauge. In such a case, one can still use the x gauge for the solution and then use the gauge transformation (B3) to bring it into the v gauge. This is the path actually followed in Sec. III B.

4. High intensity, temporal overlap with laser pulse

Figure 4 illustrates the second scenario. Here, we use the v gauge throughout and compare the raw scheme (6) with the PA scheme (14). The lowest panel shows the laser profile (15) together with the squared wave function $|\psi(z_{\mathcal{M}},t)|^2$ at the measuring point. This signals a critical situation where the laser is fully active while the wave packet is passing by the measuring point. The three upper panels show results for different intensities. The raw recipe still works acceptably well for the moderate intensity $I = 10^{12}$ W/cm^2, but becomes

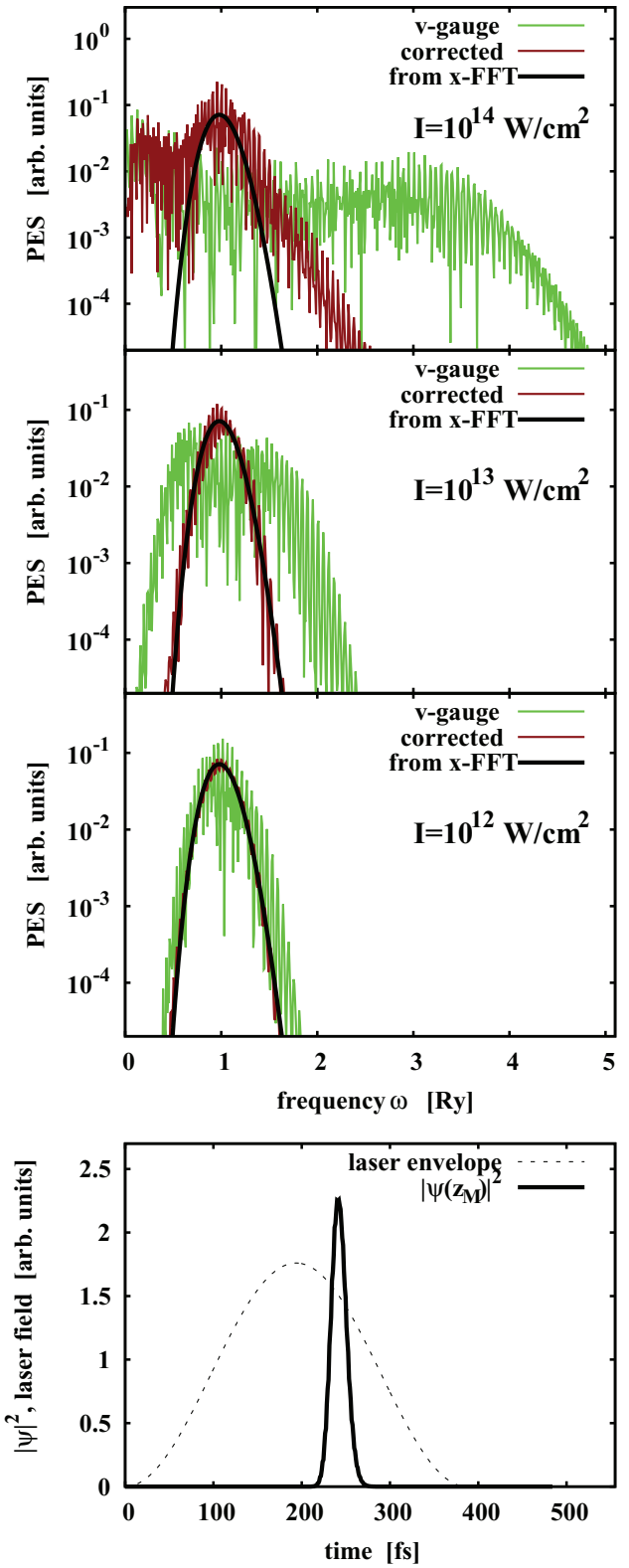

FIG. 4. (Color online) Photoelectron spectra from wave-packet analysis. Lower panel: the laser pulse envelope (dashed line) and the probability density $|\psi(z_{\mathcal{M}},t)|^2$ at the measuring point (full line). Upper panels: PES analysis at $z_{\mathcal{M}}$ in the v gauge from raw (green or light gray curve) and PA (brown or dark gray line) schemes for three laser intensities as indicated in each panel. For comparison, the momentum distribution of the wave packet from the direct scheme as given in Eq. (17) is also shown (black thick curve).

grossly misleading for higher intensities. Again, in order to scale these values to typical physical systems, let us consider the case of small sodium clusters, later computed in this work. A laser intensity in the 10^{12} W/cm^2 range leaves the system to a large extent still "intact", while intensities in the 10^{13-14} W/cm^2 may easily lead to a complete stripping of electrons from such clusters. The PA scheme (14) visibly improves the performance. The results become reliable up to $I = 10^{13}$ W/cm^2 and remain somehow qualitatively correct for the highest intensity. It is thus much more preferable to use the phase-augmented form (14) for the evaluation of the PES.

5. *High intensity, no temporal overlap with laser pulse*

Figure 5 shows results from the third scenario, where the measuring point has been moved farther away to $z_{\mathcal{M}} = 2000\,a_0$ which decouples the laser pulse from the wave packet's signal. The case of highest intensity $I = 10^{14}$ W/cm^2 is shown. As expected, the raw recipe in the v gauge yields the same result as the PA one in the same gauge, and both nicely agree with the result obtained within the direct scheme. Moreover, the x gauge (not shown here) yields precisely the same result as the v gauge. Thus, all distinctions and considerations are unnecessary in the case where laser pulse and particle flow do not overlap.

B. Realistic test cases

As a first realistic test case, we come back to the introductory example of Fig. 1, namely, the cluster Na_9^+. We take the laser with a typical infrared frequency and two rather large intensities. The axial symmetry of this and of the following example allows us to perform the calculations in cylindrical coordinates. Figure 6 shows the results for the raw and the PA recipes. The raw PES in the upper panel repeats the case of Fig. 1 showing the unexpected high-energy shoulder. The PA PES makes a dramatic difference. It shows a reasonable, almost monotonous, decrease of the envelope. Only at about 2.5 Ry, the decrease turns into a rather weak slope which may be unrealistic as we come here into a region of very low yield where unwanted background may spoil the analysis. Mind nevertheless that this background is about five orders of magnitude suppressed as compared to low-energy signals. The next lower intensity (lower panel) already shows reasonable pattern with the raw scheme. The PA scheme brings some improvement as it removes the glimpse of a shoulder at about

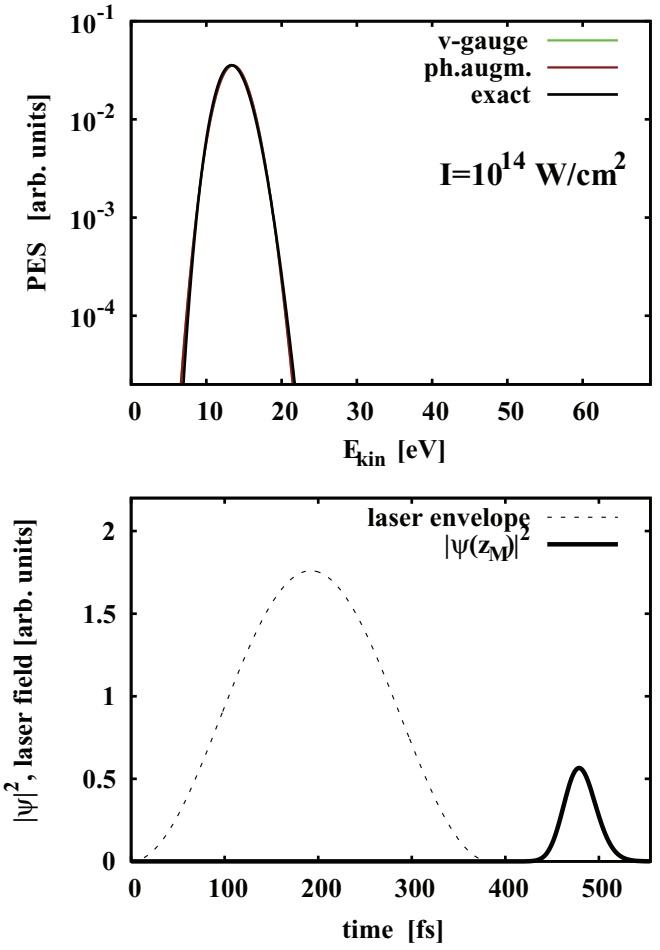

FIG. 5. (Color online) As in Fig. 4, but for a situation where the laser pulse does not overlap with the wave packet at the measuring point (see bottom panel). Only the case of strongest laser intensity is shown.

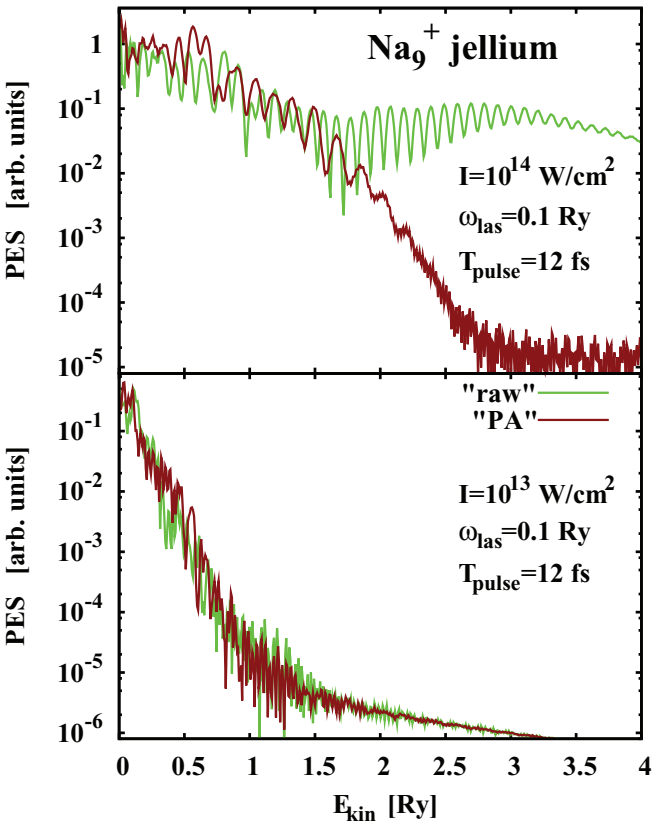

FIG. 6. (Color online) Ionization properties for Na_9^+ with jellium background under the influence of a laser pulse having frequency $\omega_{las} = 0.1$ Ry, pulse length $T_{pulse} = 12$ fs, and intensity as indicated in each panel, computed in a cylindrical box of $176 \times 88 a_0^2$ with spherical absorbing bounds covering at least 16 grid points. The laser field was given effectively in the v gauge. The raw results (green or light gray curves) are given by Eqs. (6), while the PA results (brown or dark gray curves) are complemented by the phase factor (13a).

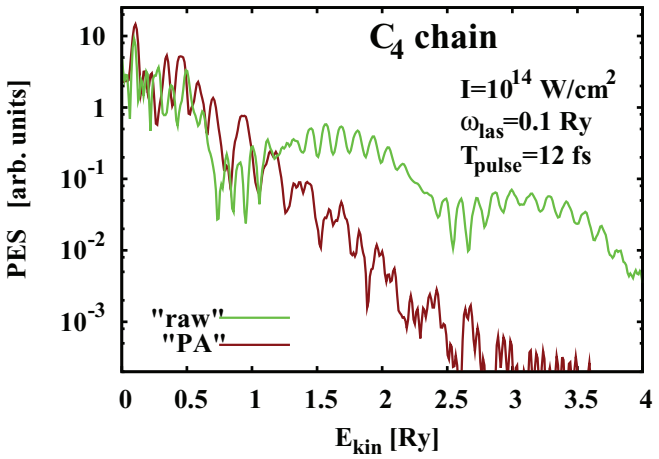

FIG. 7. (Color online) Ionization properties for the C_4 chain under the influence of a laser pulse having frequency $\omega_{las} = 0.1$ Ry, pulse length $T_{pulse} = 12$ fs, and intensity as indicated. The laser field was given effectively in the v gauge. The raw results (green or light gray curve) are given by Eqs. (6), while the PA results (brown or dark gray line) are complemented by the phase factor (13a).

1.1 Ry. As already observed in the analytic case of a Gaussian wave packet, lower intensities perform already well with the raw scheme and the difference brought in from the PA scheme is negligible.

Figure 7 shows a next test case result for the C_4 chain, treated with nonlocal pseudopotentials of Goedecker type [25] and, again, the electronic energy-density functional of Ref. [22]. The unphysical shoulders obtained with the raw scheme are even more developed than in the case of Na_9^+, and their successful removal by the PA scheme is impressive. This is a clear demonstration of the gain achieved by the PA scheme (14).

The tests show that the phase-augmented recipe allows an analysis of PES for higher laser intensities than before, typically at least more than one order of magnitude. It will, of course, also be limited by the approximations involved, such as $k = \sqrt{2\omega}$ in Eq. (13a), or the fact that only the laser field is present at the measuring point. Very little can be said in general because the limitations depend on the details of the actual test case, as the ionization potential of the cluster, possible resonant amplification, or size of the numerical box. The discussion of the PA recipe in Sec. II B4 gives an idea about an estimate related to the curvature of the phase δq. But, the most practical test is to run a calculation for different box sizes. Artifacts will be signified by a strong box dependence. It remains a topic for further research to gather more experience with cases of failure.

IV. CONCLUSIONS

In this work, we have investigated a scheme for a nonperturbative evaluation of photoelectron spectra (PES) in connection with time-dependent density-functional theory treated on a coordinate-space grid. We have extended an existing, simple evaluation scheme to the regime of high laser intensities. The original method (raw scheme) was based on the assumption of freely propagating outgoing waves at a measuring point close to absorbing boundaries. This requires negligible potentials at the measuring point. For high laser intensities, however, this assumption of free-electron motion becomes questionable. In order to extend the applicability of the scheme for evaluating PES to stronger fields, we have considered the motion of a free particle plus an external laser field in dipole approximation. This case is still analytically solvable and the analytical solution allows us to deduce a generalized scheme for evaluating PES. It consists in augmenting the wave function collected at the measuring point by an appropriate phase factor accounting for the time-dependent laser field. The coincidence of the laser field with the outgoing electron wave at the measuring point requires that we also investigate the effect of gauge transformations on the results and ponder the question of the most appropriate choice of gauge. We have found that the appropriate gauge for evaluating PES is clearly the v gauge (velocity gauge). Still, the most practical way to produce the wave functions in the v gauge is to compute them first in the x gauge (space gauge) and to apply then the appropriate gauge transformation.

The generalized scheme ("phase-augmented" recipe) has been tested in an analytical model of Gaussian wave packets and in a few realistic examples. A major result is that the original scheme for PES is valid for low and moderate laser fields (about 10^{12} W/cm^2 for the test case Na_9^+). It remains valid in the case that the particle flow arrives at the measuring point after the laser pulse has died out (in this case for all intensities). The generalized scheme was shown to considerably extend the range of applicability. The gain was particularly dramatic for the example of the C_4 chain. Moreover, we have been able to check laser intensities up to 10^{14} W/cm^2 for our realistic test cases, which all involved a low laser frequency of 0.1 Ry. Higher laser frequencies reduce the effective intensity (Keldysh criterion). Thus, even higher intensities may be used for higher frequencies.

After the promising tests reported in this work, this generalized scheme for evaluating PES is ready to be used in more demanding situations such as molecular systems with large ionization potentials, e.g., N_2, C_{60}, or typical organic molecules, for which experimental data already exist.

ACKNOWLEDGMENT

This work was supported by Institut Universitaire de France, Agence Nationale de la Recherche, and the Humboldt foundation.

APPENDIX A: THE RAW RECIPE IN 3D

As in 1D, we assume for the 3D case free propagation and purely outgoing waves at the measuring point $\mathbf{r}_{\mathcal{M}}$. The solution of the one-particle time-dependent Schrödinger equation in free space reads as

$$\psi(\mathbf{r},t) = \int \frac{d^3\mathbf{k}}{\sqrt{(2\pi)^3}}\, g(\mathbf{k})\, e^{i(\mathbf{k}\cdot\mathbf{r}-\omega t)}. \tag{A1}$$

Analogously to the 1D case, we calculate the unperturbed wave function $\widehat{\psi}_0(\mathbf{k})$ from the Fourier transform in frequency space of $\psi(\mathbf{r},t)$, assuming that only wave vectors $\mathbf{k} = k\,\mathbf{e}_\mathbf{r}$ with $k > 0$ contribute, where $\mathbf{e}_\mathbf{r}$ is the direction of the outgoing

radial wave. This yields

$$\widehat{\psi}_{0,\Omega_{\mathbf{r}}}(\mathbf{k}) \propto \widetilde{\psi}(\mathbf{r},\omega), \tag{A2}$$

where $\Omega_{\mathbf{r}}$ is the solid angle related to the $\mathbf{r}$ direction. Considering $\mathbf{r}_{\mathcal{M}}$ as the measuring point, we compute the PES in direction $\Omega_{\mathbf{r}_{\mathcal{M}}}$ as

$$\mathcal{Y}_{\Omega_{\mathbf{r}_{\mathcal{M}}}}(E_{\rm kin}) \propto |\widetilde{\psi}(\mathbf{r}_{\mathcal{M}},E_{\rm kin})|^2. \tag{A3}$$

The above analysis yields the fully energy- and angular-resolved PES. The angular-averaged PES would then be attained by angular integration with proper solid-angle weights. It has nevertheless to be emphasized that the resulting angular dependence in the laboratory frame depends on the orientation of the molecule (or cluster). Actual ensembles in the gas phase do not contain molecules in well-defined orientation but represent rather an equidistribution of all possible orientations. Typical examples are the many recent measurements of angular-resolved PES in cluster physics (see, e.g., [26–30]). An appropriate orientation averaging has to be performed before one can compare $\mathcal{Y}_{\Omega_{\mathbf{r}_{\mathcal{M}}}}(E_{\rm kin})$ with experimental data. The practical procedures for that are outlined in Refs. [31,32]. Orientation averaging, however, is beyond the scope of this paper and will be ignored in the following.

APPENDIX B: CHANGING GAUGE

In Sec. II B1, we have introduced the x gauge with the fields (8) and the v gauge with the fields (9). Both gauges are equivalent. They are connected by a gauge transformation which in general reads as

$$\Phi' = \Phi + \frac{\dot{\chi}}{c}, \tag{B1a}$$

$$\mathbf{A}' = \mathbf{A} - \boldsymbol{\nabla}\chi, \tag{B1b}$$

$$\psi' = \psi \exp\left(\frac{\mathrm{i}\chi}{c}\right), \tag{B1c}$$

where χ is a differential, but otherwise arbitrary, function of z and t. Let us assume that we take the v gauge as a starting point: the laser field is described by the potentials in Eq. (9). If we want to gauge transform the vector potential into the scalar potential, then $\boldsymbol{\nabla}\chi = \mathbf{A}^{(v)}$, from where

$$\chi = -cE_0F(t)z \quad \Rightarrow \quad \Phi^{(x)} = \frac{\dot{\chi}}{c} = -E_0 f(t)z. \tag{B2}$$

The complementing transformation for the wave functions reads as

$$\psi^{(x)} = \psi^{(v)} \exp[-i E_0 F(t) z], \tag{B3}$$

which relates the wave function $\psi^{(x)}$ as computed by time propagation under the action of the scalar potential (8), and $\psi^{(v)}$ for the case with the vector potential (9). It is obvious that this phase factor is crucial in the present PES analysis, while it can easily be ignored for local observables as, e.g., dipole momentum or net ionization.

The phase transformation allows one to decouple the gauge used in the analysis from that used in the time evolution. Assume that we solve the Schrödinger equation using the potentials (9). This immediately yields the wave function $\psi^{(v)}$ in the v gauge. The same wave function could be obtained by using Eq. (8) and applying the reverse transformation (B3) to recover $\psi^{(v)}$ from the $\psi^{(x)}$ as obtained by propagation. In fact, this is the most efficient way to evaluate $\psi^{(v)}$ as the operator (8) is purely local. It is to be noted that the transformation (B3) is relevant for the PES only if the outgoing wave reaches the measuring point $z_{\mathcal{M}}$ at a time where the signal $F(t)$ is still active. If the outgoing wave and the signal can avoid to coincide, each gauge yields the same result.

APPENDIX C: SOLUTION OF THE SCHRÖDINGER EQUATION FOR THE WAVE-PACKET MODEL

We provide the analytical solution of the wave-packet propagation in the x gauge. This is simpler and the v gauge is easily regained by the phase transformation (B3). The starting point is the following Schrödinger equation:

$$\left[\frac{\hat{\mathbf{p}}^2}{2} + E_0 z f(t)\right] \psi^{(x)}(z,t) = i\partial_t \psi^{(x)}(z,t), \tag{C1a}$$

$$\psi^{(x)}(z,0) = \psi_0^{(x)}(z), \tag{C1b}$$

$$f = \partial_t F. \tag{C1c}$$

The ansatz for the solution is given by

$$\psi^{(x)}(z,t) = \left(\frac{\mu_0}{\pi\,\mu^*(t)\mu(t)}\right)^{1/4} \times \exp\left(ip(t)z - \frac{[z-q(t)]^2}{2\mu(t)} - i\Omega(t)\right) \tag{C2}$$

with $\mu(t) = \mu_0 + i\xi t$. The other time-dependent parameters are determined substituting (C2) in the time-dependent Schrödinger equation and comparing term by term. In order to achieve this we first build the necessary derivatives:

$$\frac{i\partial_t\psi}{\psi} = -\frac{i}{2}\frac{\xi^2 t}{\mu_0{}^2+\xi^2t^2} - \dot{p}z + \frac{i\dot{q}}{\mu}(z-q) - \frac{\xi}{2}\frac{(z-q)^2}{\mu^2} + \dot{\Omega},$$

$$\hat{p}\psi = \left(p + \frac{i}{\mu}(z-q)\right)\psi,$$

$$\frac{\hat{p}^2\psi}{2\psi} = \frac{p^2}{2} + \frac{ip}{\mu}(z-q) + \frac{\mu_0 - i\xi t}{2(\mu_0{}^2+\xi^2t^2)} - \frac{1}{2}\frac{(z-q)^2}{\mu^2},$$

$$\frac{\Phi\psi}{\psi} = -E_0 z f(t).$$

Identifying term by term, we obtain the following equations for the parameters

$$(z-q)^2 : \xi = 1, \quad (z-q) : \dot{q} = p,$$
$$z : \dot{p} = -E_0\, f(t), \quad t : \xi^2 = \xi,$$
$$z^0 : \dot{\Omega} = \frac{p^2}{2} + \frac{\mu_0 - i\xi t}{2(\mu_0{}^2+\xi^2t^2)} + \frac{i\xi^2 t}{2(\mu_0{}^2+\xi^2t^2)}$$

from which one gets

$$\mu = \mu_0 + it, \tag{C3a}$$

$$p = p_0 - E_0F(t), \quad F(t) = \int_0^t dt'\, f(t'), \tag{C3b}$$

$$q = q_0 + p_0 t - E_0 \int_0^t dt'\, F(t'), \tag{C3c}$$

$$\begin{aligned}\Omega &= \Omega_0 + \frac{1}{2}\int_0^t dt' \left(p^2 + \frac{\mu_0}{{\mu_0}^2 + t^2}\right) \\ &= \Omega_0 + \frac{{p_0}^2}{2} t - p_0 E_0 \int_0^t dt'\, F(t') \\ &\quad + \frac{{E_0}^2}{2}\int_0^t dt'\, F^2(t') + \frac{1}{2}\mathrm{atan}\left(\frac{t}{\mu_0}\right).\end{aligned} \tag{C3d}$$

Using now the gauge transformation (B3), the wave function in the v gauge becomes

$$\begin{aligned}\psi^{(v)}(z,t) = &\left(\frac{\mu_0}{\pi({\mu_0}^2 + t^2)}\right)^{1/4} e^{ip_0 z} \\ &\times \exp\left(-\frac{[z - q(t)]^2}{2(\mu_0 + it)} - i\Omega(t)\right).\end{aligned} \tag{C4}$$

[1] D. W. Turner and M. I. A. Jobory, J. Chem. Phys. **37**, 3007 (1962).
[2] D. Turner, *Molecular Photoelectron Spectroscopy* (Wiley, New York, 1970).
[3] P. Ghosh, *Introduction to Photoelectron Spectroscopy* (Wiley, New York, 1983).
[4] K. M. McHugh, J. G. Eaton, G. H. Lee, H. W. Sarkas, L. H. Kidder, J. T. Snodgrass, M. R. Manaa, and K. H. Bowen, J. Chem. Phys. **91**, 3792 (1989).
[5] J. Rabalais, *Principles of Ultraviolet Photoelectron Spectroscopy* (Wiley, New York, 1977).
[6] J. Moulder, W. Stickle, P. Sobol, and K. Bomben, *Handbook of X-ray Photoelectron Spectroscopy* (Perkin-Elmer Corp., Eden Prairie, MN, 1962).
[7] G. Geloni, E. Saldin, L. Samoylova, E. Schneidmiller, H. Sinn, T. Tschentscher, and M. Yurkov, New J. Phys. **12**, 035021 (2010).
[8] C. Bressler and M. Chergui, Annu. Rev. Phys. Chem. **61**, 263 (2010).
[9] A. Pietzsch, A. Fhlisch, M. Beye1, M. Deppe, F. Hennies, M. Nagasono1, E. Suljoti, W. Wurth, C. Gahl, K. Dbrich, and A. Melnikov, New J. Phys. **10**, 033004 (2008).
[10] L. H. Tjeng, A. R. Vos, and G. A. Sawatzky, Surf. Sci. **235**, 269 (1990).
[11] M. A. Hoffmann, G. Wrigge, B. v Issendorff, J. Muller, G. Gantefor, and H. Haberland, Eur. Phys. J. D **16**, 9 (2001).
[12] H. Liu and R. J. Hamers, Surf. Sci. **416**, 354 (1998).
[13] F. H. M. Faisal, *Theory of Multiphoton Processes* (Plenum, New York, 1987).
[14] A. Pohl, P.-G. Reinhard, and E. Suraud, Phys. Rev. Lett. **84**, 5090 (2000).
[15] A. Pohl, P.-G. Reinhard, and E. Suraud, J. Phys. B: At., Mol. Opt. Phys. **34**, 4969 (2001).
[16] U. De Giovannini, D. Varsano, M. A. L. Marques, H. Appel, E. K. U. Gross, and A. Rubio, Phys. Rev. A **85**, 062515 (2012).
[17] A. Pohl, P.-G. Reinhard, and E. Suraud, Phys. Rev. A **68**, 053202 (2003).
[18] A. Pohl, P.-G. Reinhard, and E. Suraud, J. Phys. B: At., Mol. Opt. Phys. **37**, 3301 (2004).
[19] P. M. Dinh, S. Vidal, P.-G. Reinhard, and E. Suraud, New J. Phys. **14**, 063015 (2012).
[20] M. Baer, P. M. Dinh, P.-G. Reinhard, and E. Suraud, J. Phys.: Conf. Series **373**, 012011 (2012).
[21] A. Rajam, P. Hessler, C. Gaun, and N. T. Maitra, J. Mol. Struct.: THEOCHEM **914**, 30 (2009).
[22] J. P. Perdew and Y. Wang, Phys. Rev. B **45**, 13244 (1992).
[23] C. Legrand, E. Suraud, and P.-G. Reinhard, J. Phys. B: At., Mol. Opt. Phys. **35**, 1115 (2002).
[24] A. Pohl, Ph.D. thesis, Friedrich-Alexander-Universität, Erlangen/Nürnberg, 2003.
[25] S. Goedecker, M. Teter, and J. Hutter, Phys. Rev. B **54**, 1703 (1996).
[26] J. Pinaré, B. Baguenard, C. Bordas, and M. Broyer, Eur. Phys. J. D **9**, 21 (1999).
[27] J. Wills, F. Pagliarulo, B. Baguenard, F. Lpine, and C. Bordas, Chem. Phys. Lett. **390**, 145 (2004).
[28] O. Kostko, C. Bartels, J. Schwobel, C. Hock, and B. v Issendorff, J. Phys.: Conf. Ser. **88**, 012034 (2007).
[29] C. Bartels, C. Hock, J. Huwer, R. Kuhnen, J. Schwöbel, and B. von Issendorff, Science **323**, 132 (2009).
[30] M. Kjellberg, O. Johansson, F. Jonsson, A. V. Bulgakov, C. Bordas, E. E. B. Campbell, and K. Hansen, Phys. Rev. A **81**, 023202 (2010).
[31] P. Wopperer, B. Faber, P. M. Dinh, P.-G. Reinhard, and E. Suraud, Phys. Lett. A **375**, 39 (2010).
[32] P. Wopperer, B. Faber, P. M. Dinh, P.-G. Reinhard, and E. Suraud, Phys. Rev. A **82**, 063416 (2010).